

# Probing Water-Electrified Electrode interfaces: Insights from Au and Pd

Graciele M. Arvelos,<sup>1</sup> Marivi Fernández-Serra,<sup>2,3</sup> Alexandre R. Rocha,<sup>4,1</sup> and Luana S. Pedroza<sup>5</sup>

<sup>1</sup>*Instituto de Física Teórica, Universidade Estadual Paulista (UNESP), São Paulo, SP 01140-070, Brazil*

<sup>2</sup>*Physics and Astronomy Department, Stony Brook University, Stony Brook, New York 11794-3800, USA*

<sup>3</sup>*Institute for Advanced Computational Science, Stony Brook, New York 11794-3800, USA*

<sup>4</sup>*Max Planck Institute for the Structure and Dynamics of Matter, 22761 Hamburg, Germany*

<sup>5</sup>*Instituto de Física, Universidade de São Paulo, SP 05508-090, Brazil*

(\*Electronic mail: luana@if.usp.br)

(Dated: 1 November 2024)

The water/electrode interface under an applied bias potential is a challenging out-of-equilibrium phenomenon, which is difficult to accurately model at the atomic scale. In this study, we employ a combined approach of Density Functional Theory (DFT) and non-equilibrium Green's function (NEGF) methods to analyze the influence of an external bias on the properties of water adsorbed on Au(111) and Pd(111) metallic electrodes. Our results demonstrate that while both Au and Pd-electrodes induce qualitatively similar structural responses in adsorbed water molecules, the quantitative differences are substantial, driven by the distinct nature of water-metal bonding. Our findings underscore the necessity of quantum-mechanical modeling for accurately describing electrochemical interfaces.

## I. INTRODUCTION

An atomistic description of the water-metal interface is important for a better comprehension of a myriad of processes such as heterogeneous catalysis,<sup>1–5</sup> corrosion resistance,<sup>6</sup> and catalytic processes in solar cells.<sup>7–9</sup> In this context, many properties that characterize the reactivity and electrochemical behavior of the interface are ultimately defined by the electronic response to external factors and perturbations, such as an applied external potential.<sup>10</sup> These properties are related to atomic arrangements determined by the orientations of water molecules, the formation of different ions at the interface, and the reactions that might occur at different potentials.<sup>11</sup>

An electrochemical cell can be modeled by two independent charge reservoirs acting as electrodes separated by an electrolytic solution. Applying an electrostatic potential difference across such a device will lead to a redistribution of charge both at the electrode interface as well as in the ions composing the electrolyte. At the microscopic level, this process results in the formation of the electric double layer (EDL), responsible for the formation and breaking of chemical bonds, as well as possible charge transfer processes and adsorption occurring at the electrode interface.<sup>8,12</sup> However, even for concentrated electrolytes, water molecules dominate this interface and understanding the water-metal interaction is a first step towards a better comprehension of the EDL.<sup>13</sup> The microscopic structure of water at the metal interface can be inferred from vibrational spectroscopy techniques combined with atomistic modelling, due to the correlation between frequencies and hydrogen bond strength.<sup>14–25</sup>

Computer simulations have been crucial in analyzing and describing these structures at the atomic level and assisting in the interpretation of experimental results.<sup>25</sup> In particular, density functional theory (DFT) has elucidated experimental questions, such as the stability of water structures adsorbed on transition metals.<sup>26–29</sup> However, modeling an electrified electrode/electrolyte interface with atomistic accu-

racy and at a reasonable computational cost is still a major challenge.<sup>9,30–35</sup> In the realm of DFT, Filhol and Neurock<sup>11</sup> implemented the electrification of a metal surface by modifying the total number of electrons on the electrode. Using this approach, the authors studied the response of the polarization of water/Pd(111) and water/Cu(111) interfaces to an external potential.<sup>11,36</sup> Other implementations in this direction have emerged in the literature over the years, providing details about the water-metal interface, polarization effects, insights into processes occurring in the EDL, and information about activation energies.<sup>37–41</sup> In all these studies, the variable that is theoretically controlled is the added (or subtracted) charge to/from the electrode, and the resulting applied potential is then inferred from the computed average electric field in the device. This does not replicate experiments, where the applied potential is the control variable, and the electrode charges depend on the response of the electrolyte to such applied bias. There were also developments in the direction of controlling the potential, using a potentiostat. However, in this approach the instantaneous potential and dynamics are not described, and what is obtained is the average potential at the electrode.<sup>42,43</sup>

Recently we have proposed<sup>44</sup> a methodology that correctly models the experimental scenario. It is based on the non-equilibrium Green's function (NEGF) formalism combined with DFT.<sup>45–48</sup> It is specifically designed to system under an external bias potential and can be readily applied to a solid-liquid interface. It has the advantage of controlling the bias considering the electrodes as semi-infinite reservoirs,<sup>34,44,49</sup> as well as obtaining the forces in an out-of-equilibrium situation with ab-initio precision.<sup>50–52</sup> In this work, we apply this methodology to describe the effect of electrically biased surfaces on water structures (monomer and a monolayer) adsorbed on two distinct metal surfaces – Au(111) and Pd(111). This allows us to quantitatively evaluate the differences between these two electrodes.

## II. COMPUTATIONAL DETAILS

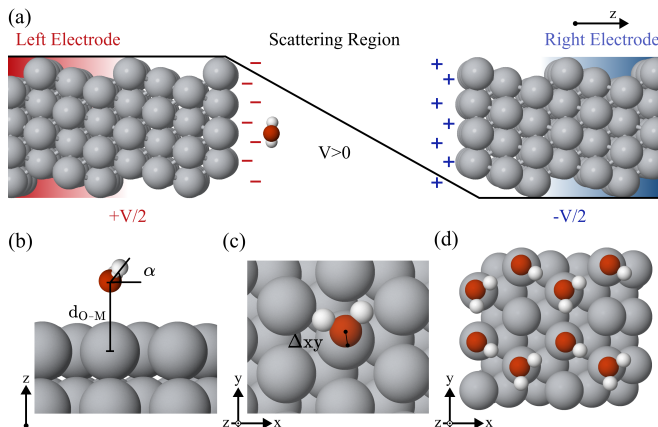


FIG. 1. (a) Illustration of the electrochemical setup in the framework of the NEGF formalism used to apply an external bias potential into the water-metal system. The LE and RE regions correspond to the left and right electrodes, respectively, and the SR is known as the scattering region; (b) side and (c) top views of a water monomer on the metallic surface and structural properties measured after optimization: the vertical distance between oxygen and metal atom ( $d_{O-M}$ ), tilt angle between metal surface and the plane formed by the molecule ( $\alpha$ ), and the horizontal displacement from the top position on the metal surface ( $\Delta_{xy}$ ), respectively; (d) top view of the H-down water layer.

For studies of the isolated water monomer, we have analyzed its structural and vibrational dependence upon bias changes in two different surfaces, Au(111) and Pd(111). We made this choice because they expand the range of water-adsorption mechanisms in noble metals. While for Au the adsorption is dominated by electrostatics, in Pd a significant amount of charge transfer at the interface occurs.<sup>26,27</sup> In addition we also analyze the behavior of a monolayer of 2D ice water adsorbed on the Au electrode. The systems considered in our simulations were composed of two semi-infinite metal slabs acting as electrodes, and the water (monomer and monolayer) in contact with one of them, as illustrated in Fig.1(a). This is similar to the arrangements used in standard electronic transport calculations. For the simulations, the system is split into three regions<sup>53</sup>, namely two semi-infinite electrodes in thermal equilibrium - albeit with a possibly different chemical potential if a bias is applied - and a so-called scattering region (SR), which consists of a water molecule/monolayer and a number of layers of metal on either side. The number of layers used ensures that the charge density at both edges of the simulation box is the same as the one deep inside the bulk electrodes.

For the gold electrodes (both for a water monomer and for a monolayer), the optimized bulk lattice constant is 4.24 Å and the system was constructed with 3 layers, each one containing  $3 \times 4$  Au atoms on the surface plane forming the leads on either side. These are then attached to four layers on the left and three layers on the right forming the full simulation cell as illustrated in Fig. 1(a). The left and right metallic sur-

faces are separated by 25 Å, and the water molecule or the 2D monolayer adsorbed on the left electrode. We have chosen a H-down layer as seen in Fig. 1(d), as this was shown to be a stable configuration.<sup>29</sup> The layer consisted of 8 water molecules in a hexagonal arrangement, similar to ice Ih, in a unit cell of size  $\sqrt{3} \times \sqrt{3}R_{30}$  relative to the lattice parameter of Au, as this makes them almost commensurate (Fig. 1(d)). In the case of the monomer adsorbed on Pd electrodes, the Pd bulk lattice constant is 3.97 Å, and again we used a layer of Pd formed by  $3 \times 4$  atoms. The electrodes now consist of 6 layers to guarantee coupling between neighboring cells only. These are again connected to four and three layers to the left and right, respectively, and the vacuum region is kept at 25 Å.

Initially we performed standard equilibrium density functional theory calculations with periodic boundary conditions (PBC) using the Siesta<sup>54</sup> code with PBE<sup>55</sup> as our choice of exchange and correlation potential (XC). The valence electrons were described by optimized numerical atomic orbitals with double- $\zeta$  polarization,<sup>27,44</sup> and the core electrons were described by norm-conserving pseudopotentials in the Troullier-Martins form<sup>56</sup>. Subsequently, a finite voltage was applied to the electrodes, shifting the left (right) chemical potentials by  $V/2$  ( $-V/2$ ) and inducing a negative (positive) charge on the surface for positive (negative) bias. Thus, the problem becomes a non-equilibrium one and the calculations were performed self-consistently using the NEGF formalism coupled with DFT with the same parameters used for the ground state calculations. For each applied bias the system is relaxed by self consistently calculating the non-equilibrium forces.<sup>44,50,51</sup> All non-equilibrium calculations were performed using the Transiesta code.<sup>47,48</sup>

The minimum energy configuration of the water monomer adsorbed on each metal was obtained with the criteria of 0.005 eV/Å for the maximum force on each atom and with the electrode atoms fixed at the bulk geometry (the metal atoms closer to the surface are allowed to move for PBC optimization). The final configuration is then used as a starting point for the next bias voltage. Using the optimized geometry, the vibrational modes for the water molecule were obtained by diagonalizing a numerically computed force constant matrix where the water atoms are displaced by 0.01 Bohr from their equilibrium positions. Parameter convergence in structural optimizations incorporating NEGF methods is critical to ensure the validity of the observed simulation results. In particular, one needs to ensure that the number of metal-electrode layers is sufficient. At zero applied bias, structural properties of adsorbents computed using a n-layers metal slab with PBC should not differ from those obtained in a NEGF simulation with semi-infinite separated electrodes. We have ensured that our results are converged using these criteria.

## III. RESULTS AND DISCUSSION

### A. Water monomer

In the absence of applied potential, for both Pd and Au surfaces, the optimal arrangement for the water monomer ad-

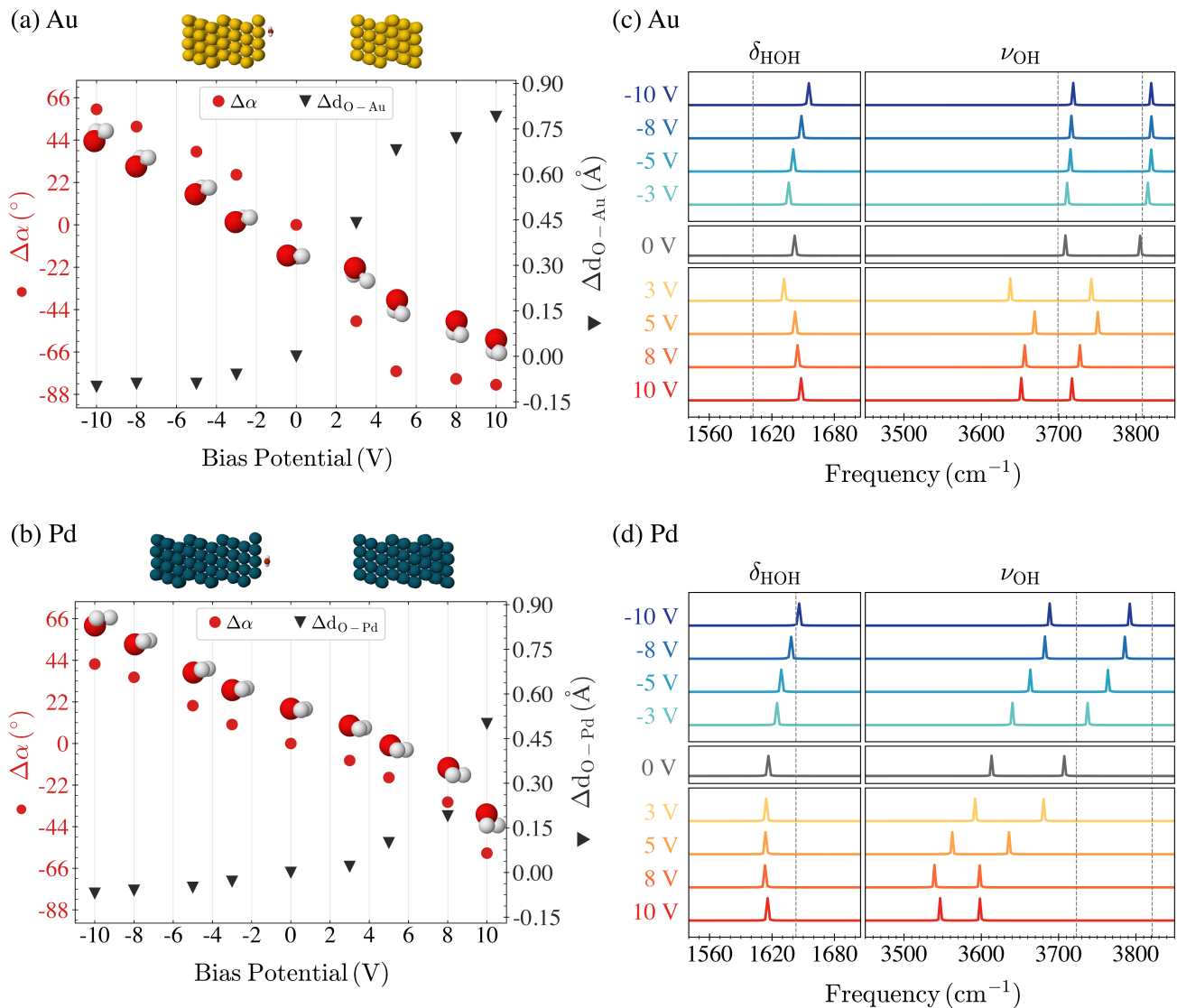


FIG. 2. Relative tilt angle and water-metal distance of a water monomer adsorbed on (a) Au(111) and (b) Pd(111) surfaces as a function of applied bias, compared to the zero-bias configuration. The bias-dependent equilibrium water configuration is also shown. (c) and (d) show the normal mode frequencies of a water molecule adsorbed on Au(111) and Pd(111) surfaces under applied bias, respectively. The dotted line represents the frequencies of an isolated water monomer, calculated with the inclusion of metal ghost atoms.

sorbed on it is a flat configuration,<sup>26,28,29,44,57–59</sup> *i.e.* the water dipole is approximately parallel to the surface as measured by  $\alpha$ , the angle between the dipole moment and its component on the  $xy$  plane (Fig. 1(b) and (c)). For Au, the bonding between molecule and surface is weaker, and the distance to the oxygen ( $d_{O-M}$ ) atom is 2.80 Å, compared to Pd which is 2.47 Å, obtained using standard periodic DFT calculations. These values are close to the values (2.83 – 3.14) Å for Au and (2.37 – 2.47) Å for Pd reported in the literature using the same XC functional.<sup>26,44,57,58</sup> We also analyzed the effects of including van der Waals corrections with the VDW-BH<sup>60</sup> exchange and correlation functional for Pd electrodes, and we obtained 2.39 Å for  $d_{O-M}$  and 2° for the tilt angle, revealing results closer to the PBE XC.<sup>26,27,58</sup> Therefore, for the calculations applying an external potential bias, we will use only

PBE. We also minimized the configuration using the NEGF-DFT methodology considering  $V = 0$  V, as can be seen from Table I for the metal-oxygen distance and the tilt angle  $\alpha$ . We note that these structural properties did not change compared to the PBC values. This indicates that the amount of metal included is sufficient for screening.

Starting from the flat configuration we applied a positive/negative external potential bias, up to 10 V (as mentioned before, the effective potential seen on any metal surface corresponds to  $V/2$  in the NEGF formalism). In Figs. 2 (a) and (b) we present the final relaxed water structure configuration as a function of the applied bias potentials as well as the distance between the metal and the oxygen, and the tilt angle for each electrode. This information is also presented in a more quantitative form in Table I.

TABLE I. Structural properties and normal mode frequencies values of a monomer adsorbed on Pd(111) and Au(111) surface according to the applied biases. We present the water-metal distance ( $d_{O-M}$ ), the water molecule tilt angle  $\alpha$  with respect to the metal surface plane, the horizontal displacement in comparison with the *atop* position along the *xy* plane ( $\Delta xy$ ), the frequencies of the bending normal mode ( $\delta_{HOH}$ ), and symmetric ( $\nu_S$ ) and antisymmetric ( $\nu_{AS}$ ) modes.

V (V)	$d_{O-M}$ (Å)		$\alpha$ (°)		$\Delta xy$ (Å)		$\delta_{HOH}$ (cm <sup>-1</sup> )		$\nu_S$ (cm <sup>-1</sup> )		$\nu_{AS}$ (cm <sup>-1</sup> )	
	Au	Pd	Au	Pd	Au	Pd	Au	Pd	Au	Pd	Au	Pd
-10	2.71	2.39	56	38	0.24	0.07	1655	1645	3718	3689	3820	3793
-8	2.72	2.40	47	31	0.17	0.07	1648	1637	3717	3683	3821	3787
-5	2.72	2.41	34	16	0.10	0.24	1640	1630	3715	3663	3820	3765
-3	2.75	2.43	22	6	0.02	0.38	1636	1624	3712	3640	3816	3738
0	2.81	2.46	-4	-4	0.35	0.49	1642	1616	3708	3614	3806	3708
3	3.25	2.51	-54	-13	1.12	0.55	1633	1614	3638	3592	3743	3683
5	3.49	2.56	-80	-22	1.38	0.67	1642	1614	3669	3552	3751	3637
8	3.53	2.65	-84	-35	1.42	0.77	1646	1614	3657	3540	3728	3599
10	3.60	2.96	-87	-62	1.55	1.02	1648	1616	3652	3547	3718	3599
Isolated monomer (Metallic Ghost Atoms)							1602	1643	3699	3723	3808	3821

In general, for both metals we observe a tendency for the oxygen (hydrogen) atom to approach (move away) the surface for  $V < 0$  and to move away (approach) from it for  $V > 0$ . This occurs due to the polarization of negative (positive) surface charge on the metal that arises when applying a positive (negative) bias to the electrodes.<sup>44</sup> In accordance with this behavior, previous studies have observed a deviation of the flat configuration to an up (down) configuration for positive (negative) metal surface polarization for Au electrodes<sup>44</sup> with NEGF formalism, as well as for a homogeneous electric field applied to a water molecule on a Pd slab.<sup>61</sup>

It is important to note that the effect of the potential is not symmetric with respect to polarity. Under a positive potential bias, the tilt angle is larger compared to that under a negative bias, which can be attributed to differences in charge transfer. As can be seen in Fig. 2(a) and Table I the structural properties of the gold electrodes are more significantly impacted due to the weaker bonding between the water molecule and the gold electrode. For example, at a relatively low bias ( $\sim 5$  V), the water molecule rotates into a downward configuration (with hydrogens pointing towards the metal), and the oxygen-metal distance ( $d_{O-M}$ ) shows minimal change as the potential increases. In contrast, on the Pd surface, the water molecule is more strongly bound, with the downward configuration occurring only at higher voltages (10V). Additionally, we observed a shift in the preferred adsorption site with positive potential, as indicated by the horizontal displacement of the water molecule ( $\Delta xy$ ). For negative bias potentials, the water favors the *atop* position, while for positive bias potentials, the *hollow* site becomes preferred.

To investigate the role of charge transfer in the bias-dependent structural properties, we calculated the overall change in the Mulliken population on the water molecule for each applied bias and compared the atomic charges to those of an isolated water monomer. As shown in Figure Figure 3, Pd exhibits a stronger charge transfer between the metal surface and the water molecule even at zero bias, which accounts for the smaller change in the oxygen-metal distance ( $\Delta d_{O-M}$ ) compared to gold. This higher charge transfer in Pd persists

across the range of applied biases, both positive and negative. Moreover, greater charge transfer occurs under negative bias

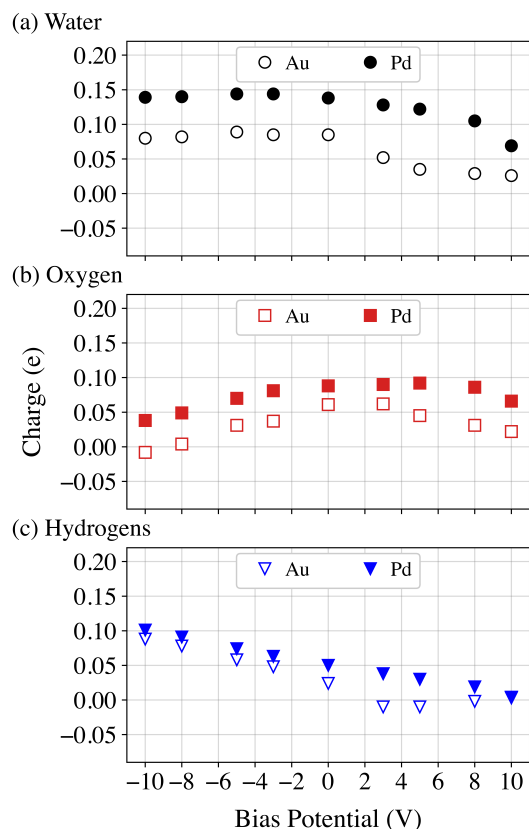


FIG. 3. Charge transfer to the water molecule in units of the electron charge for different applied bias potentials measured by Mulliken charge population for Au (empty points) and Pd (filled points) electrodes. (a) The black circles correspond to the total water charge, and the (b) red circles and (c) blue triangles represent the O and H net charge contributions compared to the isolated water monomer.

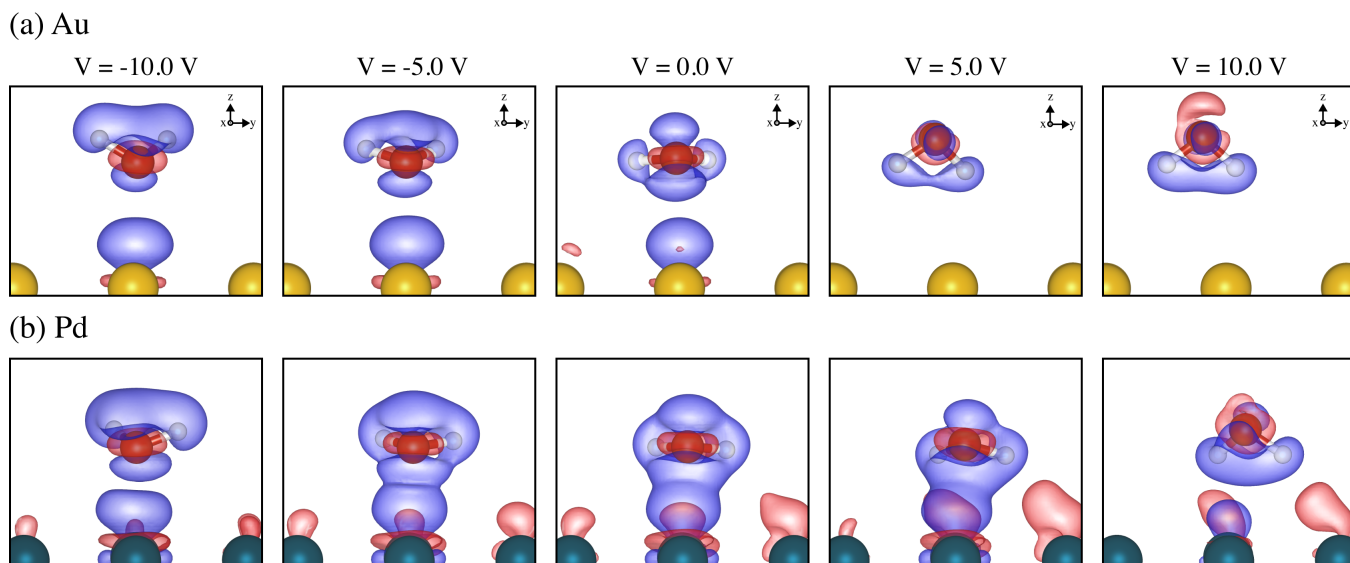


FIG. 4. Difference in charge density between the system under bias  $V$  and a combined parallel-plate capacitor with the same bias, and an isolated water molecule with an equivalent external electric applied. The isosurface value was  $1.5 \times 10^{-3} e/\text{\AA}^3$  for all plots, where red (blue) indicates an excess (depletion) of electrons.

potentials when the water molecule adopts an almost upright configuration and in the *atop* site position, in such way that is favored by the interaction between the oxygen and the metal atoms. This behaviour is reflected in the difference in charge density between the full system at a given bias and the combination of a parallel plate capacitor with bias  $V$  and an isolated molecule in an equivalent electric field (see Figure 4 and Figures S1 and S2 in the supplemental information file). This allows us to analyze the water-metal interactions excluding a classical electrostatic effect. We note that for zero bias we have the characteristic charge density profile associated to Pauli repulsion in molecule-metal systems.<sup>13,59</sup> As the bias negatively increases, Pauli repulsion increases as the oxygen atom moves closer to the surface, a competing effect of the attractive interaction between the positively charged surface and the negatively charged O atom. It is also interesting to point out that the total charge transfer between surface and molecule is small for negative bias, while there is some degree of charge rearrangement within the water molecule.

The structural changes and charge transfer induced by variations of the external potential can be reflected in the vibrational properties of the system. These have been observed experimentally using surface-enhanced infrared absorption spectroscopy (SEIRAS),<sup>22</sup> which showed modifications in the vibrational mode of angular deformation and an increase in the number of hydrogen bonds, for positive voltages. Additionally, sum-frequency generation (SFG) spectroscopy, sensitive only to the water-metal interface, revealed variations in higher-frequency OH stretching due to potential changes, attributing these shifts to free OH bonds oriented towards the gold electrode. They also observed a weak interaction of these molecules with the metal,<sup>18,19,21</sup> as well as a tendency for water molecules to move closer to the electrode under positive potentials and further away under negative potentials, ev-

idenced by an increase in interfacial water density for positive bias.<sup>21</sup>

To gain deeper insight, we first examined the behavior of a single water molecule on the surface. Thus, we have calculated the vibrational modes of the molecule as a function of the applied external potential. In the zero-bias case, the stretching frequencies,  $\nu_{OH}$ , of the water molecule adsorbed on Au are higher than those on Pd. This difference is due to the weaker binding of the molecule to the Au surface, which keeps the water molecule at a greater distance from the surface compared to Pd. In contrast, the stronger binding to Pd results in lower stretching frequencies, reflecting the closer proximity and stronger interaction between the water molecule and the Pd surface.

In the case of Pd, applying a negative external potential resulted in a significant increase in the antisymmetric stretching frequencies,  $\nu_{AS}$ , by up to  $85 \text{ cm}^{-1}$  at  $V = -10.0 \text{ V}$ . In contrast, when the molecule is adsorbed at the gold surface, we observed that  $\nu_{AS}$  increased only slightly and then remained essentially constant up to  $15 \text{ cm}^{-1}$  for negative potentials. This increase in frequencies for both surfaces is due to a reduced interaction between the O-H bonds and the metal, caused by the rotation of the water molecules away from the surface. For positive potentials ( $V > 0$ ), the stretching frequencies tend to decrease as the O-H bonds move closer to the metal surface, with a maximum reduction of  $109 \text{ cm}^{-1}$  for Pd and  $88 \text{ cm}^{-1}$  for Au. These results are in agreement with those obtained by Fidanyan *et al.*<sup>61</sup> who applied an external homogeneous electric field perpendicular to a Pd slab. While a one-to-one correspondence between field and potential is not straightforward, within the field range of  $\pm 0.44 \text{ V/\AA}$ —which corresponds to similar values as in our study—the frequencies follow the same trend of increasing with negative polarization and decreasing with positive polarization of the metal surface.

Overall, we notice that both metallic surfaces exhibit similar trends within the applied potential range, though Pd electrodes show more pronounced frequency variations for relatively smaller structural changes compared to Au.

## B. Water monolayer

The monomer adsorbed on the metal surface can be viewed as a prototype system for understanding the water-metal interactions. However, SFG experiments actually probe water layers at the interface. Therefore, we also analyzed the vibrational frequencies of a water monolayer adsorbed on the Au(111) surface as a function of the applied bias. As shown in Fig. 1(d), the hexagons in this 2D layer are formed by alternating flat and H-down (dangling H atoms pointing towards the metal electrode) molecules. Under positive bias, the flat water molecules tend to move away from the metal surface, while under negative potentials, they move closer, as shown in Figure 5. The H-down molecules remain more tightly bound, with only minimal structural changes. The average maximum deviation for the tilt angle  $\overline{\Delta\alpha}$  was just  $3^\circ$ , and for the vertical displacement  $\overline{\Delta d_{O-Au}}$  was only  $0.09 \text{ \AA}$  (see Figure S4 in the SI). This behavior of the flat water molecule is in line with the results observed for the monomer, though the variations in tilt angle and oxygen-metal distance are smaller in the monolayer. This can be attributed to the formation of hydrogen bonds between the water molecules.

The asymmetric response of the system to the sign of the applied potential is still noted, and for negative potentials, there is a larger variation of the oxygen-oxygen distance ( $\overline{\Delta d_{O-O}}$ ), whereas for positive bias the distances do not change as much with increasing potential (see SI, Figure S5). Furthermore, the effect of the external potential mostly affects the flat water molecules, as their interaction with the metal surface is stronger through the oxygen orbitals. This was also observed in *ab-initio* molecular dynamics simulations on Pt(111) and Au(111) surfaces<sup>62-65</sup> using different techniques

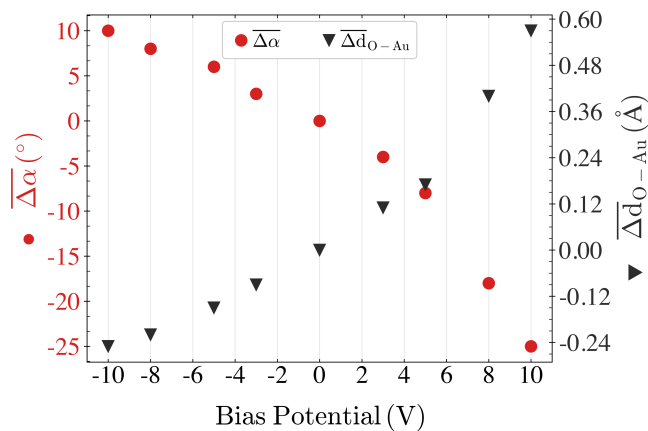


FIG. 5. Averaged tilt angle ( $\overline{\Delta\alpha}$ ) and vertical displacement ( $\overline{\Delta d_{O-Au}}$ ) variations of flat molecules in the minimum energy geometry of the water layer in each bias after the optimization.

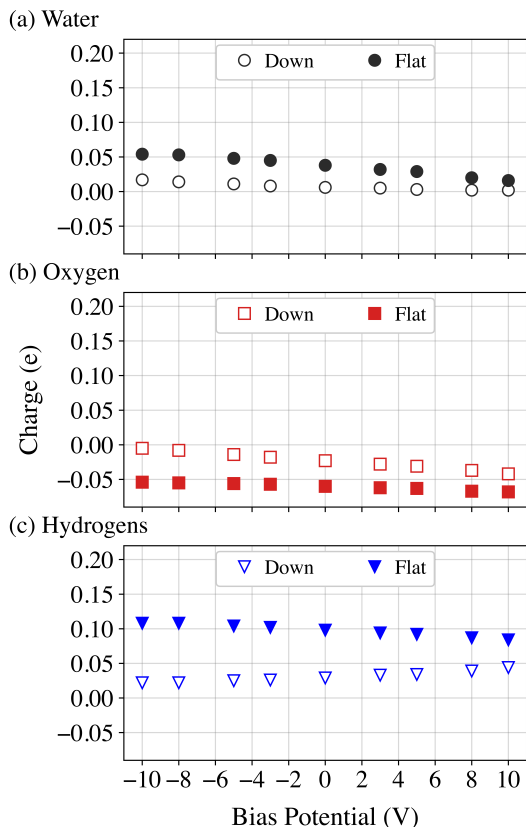


FIG. 6. Averaged charge transfer of down (empty points) and flat (filled points) water molecules. (a) The black circles correspond to the total water charge; the (b) red squares and (c) blue triangles correspond to the O and H atom contributions.

to try to mimic the external bias potential. In all cases, the interfacial water chemisorbs on the metal surface through the oxygen atom. In these studies, the authors also reported an excess of charge in the first water layer and a structural reordering of the subsequent water layers. However, the charge transfer observed in our calculations was small, indicating a weaker interaction between the water molecules and the metal electrode (see Figure 6). Moreover, the  $\sqrt{3} \times \sqrt{3}R30$  water layer arrangement limits interaction between the metallic orbitals of non-atop site atoms and the water molecules. The presence of hydrogen bonds in the monolayer further restricts the influence of these orbitals, which could otherwise facilitate charge transfer (see SI, Figure S6).<sup>8,66</sup>

Finally, the distribution of the bending and stretching modes is shown in Figure 7. To associate specific frequency values with their corresponding interactions, we analyzed the eigenvector directions for characteristic modes (see SI, Figure S8). The lower bending frequencies are associated to the flat-down molecules, while the higher-frequency vibrations are dominated by the flat-lying molecules. On the other hand, the lower stretching values correspond to the symmetric stretching modes of the molecules. For the negative potentials, the interaction between the flat-down molecules and the metal dominates these mode frequencies. As the bias in-

creases, the frequencies correspond to the hydrogen bond interaction. Intermediate frequencies correspond to a combination of symmetric stretching modes of flat molecules and

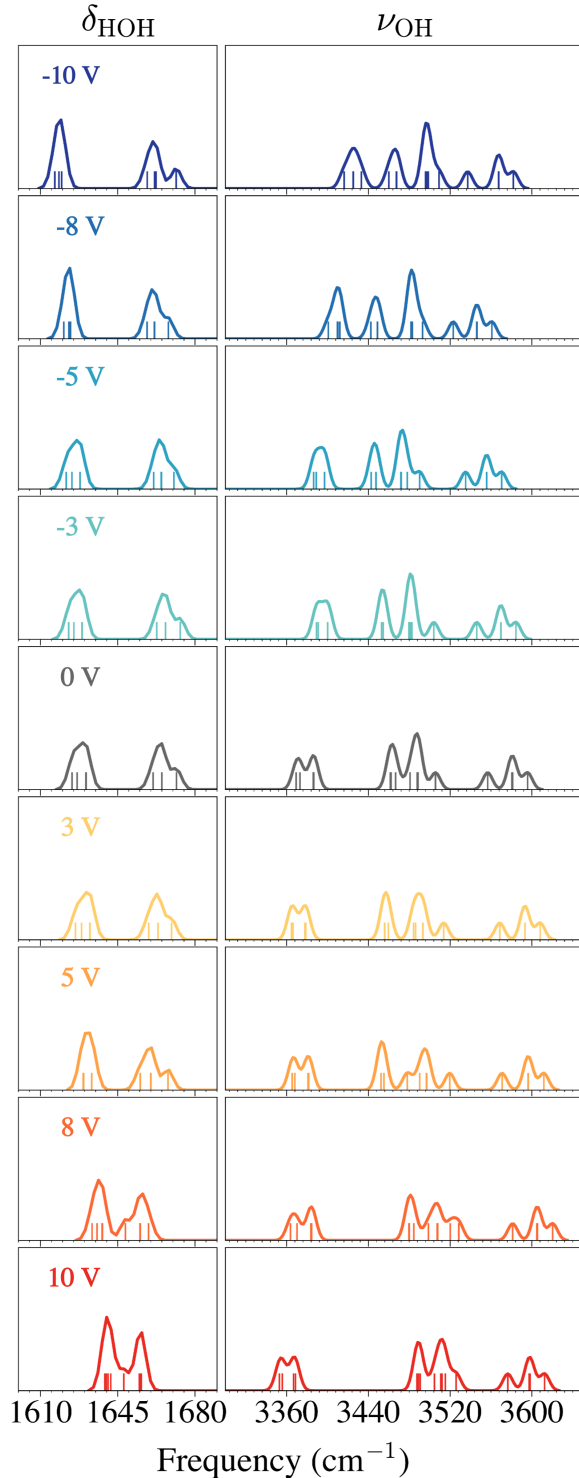


FIG. 7. Normal mode frequencies of a water monolayer adsorbed on an Au(111) surfaces for different applied bias potentials. Left handside panels correspond to bending modes, and right handside panels to stretching modes.

asymmetric stretching modes of flat-down molecules. The higher frequencies are associated with the asymmetric stretching vibrations of flat molecules.

Since there was no reorientation molecule, the stretching modes exhibit a monotonic behavior with bias, albeit with different trends. We observed that the lower frequencies tend to decrease with increasing bias, while the higher-frequency modes increase. These shifts, associated with the increase in the O-O distance of the flat-down molecule –acting as a hydrogen bond donor– result in stronger hydrogen bonds and weaker water-metal interactions (see Figure S8), as we expected from the charge transfer analysis. These results are in line with the experimental observations using shell-isolated nanoparticle-enhanced Raman spectroscopy, where an increase in stretching frequencies was observed for interfacial water on negatively charged surfaces, while higher stretching values were reported for positively charged surfaces.<sup>23,24</sup> On the other hand, the bending frequencies show an opposite trend compared to the stretching ones, where we observe a separation of the peak frequencies for negative values and an assemble for positive potentials. In this sense, for positive potentials, we observed an increase in the bending frequencies associated with the flat-down molecules and a decrease in those of the flat molecules. This result suggests stronger hydrogen bonds and weaker water-metal interactions, as the molecules are further from the metal.<sup>67</sup>

#### IV. CONCLUSION

In conclusion, we employed a combination of density functional theory (DFT) and non-equilibrium Green's functions (NEGF) to investigate the structural and vibrational properties of a water molecule on Au(111) and Pd(111) surfaces, as well as a water monolayer on Au(111). Our approach allowed us to explicitly simulate a bias voltage drop within the grand-canonical ensemble, without the need of fictitious counter-electrodes.

For a single water molecule adsorbed on metallic surfaces, we found that under negative bias, the molecule moves closer to the surface, as the surface gets positively charged and interacts more strongly with the electronegative oxygen atom. Interestingly, we note that this does not result in significant charge transfer between surface and molecule, only charge rearrangements. Moreover, the interaction is not purely electrostatic, and a competition with Pauli repulsion arises. On the other hand, the molecule tends to rotate to the down configuration for positive bias voltages. The overall structural changes are more pronounced in Au compared to Pd, as the molecule is more strongly bound to the latter - and consequently, a higher charge transfer is seen. These structural changes were reflected on the vibrational frequencies with a non-monotonic behavior for the stretching modes. These changes reflect the molecule's rotation due to the charged surface, which, in turn, strengthens or weakens the O-H bonds. Thus, the molecule binds more strongly to the metal for positive potentials via the interaction between the H atoms and the negatively charged surface. On the other hand, for negative voltages, the H atoms

move away from the positively charged surface and, as a result, interact less with the metal, leading to strengthened O-H bonds.

In the case of the water monolayer on Au(111), the presence of hydrogen bonds limits large structural changes, with the external bias primarily affecting the oxygen-metal distance. The vibrational modes present can be separated into two families ascribed to flat and flat-down molecules, respectively. For the stretching modes the frequencies tend to get closer together as the bias is increased, whereas the opposite trend is noted for the bending modes. We also observed higher stretching frequencies at positive potentials, indicating that the O-H bonds in the flat-down molecules become weaker while the hydrogen bonds strengthen. Overall, our results suggest that the monolayer binds more strongly to the surface under negative bias and more weakly under positive bias, reflecting the dynamic interplay between water-metal interactions and hydrogen bonding at the interface.

Although the systems analysed in this work can be viewed as prototypes, this work provides new insights into the complex behavior of water adsorbed on electrified surfaces. Also, the configurations examined here can be used to train neural network-based force fields for modeling water/metal interfaces under bias, paving the way for more accurate and computationally efficient atomistic simulations.

## ACKNOWLEDGMENTS

The authors would like to acknowledge financial support from Fundação de Amparo à Pesquisa do Estado de São Paulo (FAPESP Grant # 2017/10292-0, 2020/16593-4, 2017/02317-2, 2023/09820-2), Conselho Nacional de Pesquisa (CNPq) and CAPES. Calculations were carried out at CENAPAD-SP and at the Santos Dumont High performance facilities of Laboratório Nacional de Computação Científica (LNCC), Brazil.

## DATA AVAILABILITY STATEMENT

The data are available from the corresponding author upon reasonable request.

- <sup>1</sup>A. J. Shih, M. C. O. Monteiro, F. Dattila, D. Pavesi, M. Philips, A. H. M. da Silva, R. E. Vos, K. Ojha, S. Park, O. van der Heijden, G. Marcandalli, A. Goyal, M. Villalba, X. Chen, G. T. K. K. Gunasooriya, I. McCrum, R. Mom, N. López, and M. T. M. Koper, *Nature Reviews Methods Primers* **2**, 84 (2022).
- <sup>2</sup>M. Li, L. Li, X. Huang, X. Qi, M. Deng, S. Jiang, and Z. Wei, *The Journal of Physical Chemistry Letters* **13**, 10550 (2022), pMID: 36342770, <https://doi.org/10.1021/acs.jpcclett.2c02907>.
- <sup>3</sup>N. Dubouis and A. Grimaud, *Chem. Sci.* **10**, 9165 (2019).
- <sup>4</sup>S. Surendralal, M. Todorova, and J. Neugebauer, *Phys. Rev. Lett.* **126**, 166802 (2021).
- <sup>5</sup>O. M. Magnussen and A. Groß, *Journal of the American Chemical Society* **141**, 4777 (2019), pMID: 30768905, <https://doi.org/10.1021/jacs.8b13188>.
- <sup>6</sup>N. R. Council, *Research Opportunities in Corrosion Science and Engineering* (The National Academies Press, Washington, DC, 2011).
- <sup>7</sup>J. Le, M. Iannuzzi, A. Cuesta, and J. Cheng, *Phys. Rev. Lett.* **119**, 016801 (2017).
- <sup>8</sup>M. T. Darby and C. S. Cucinotta, *Current Opinion in Electrochemistry* **36**, 101118 (2022).
- <sup>9</sup>K. Schwarz and R. Sundararaman, *Surface Science Reports* **75**, 100492 (2020).
- <sup>10</sup>J. Carrasco, A. Hodgson, and A. Michaelides, *Nature Materials* **11**, 667 (2012).
- <sup>11</sup>J.-S. Filhol and M. Neurock, *Angewandte Chemie International Edition* **45**, 402 (2006), <https://onlinelibrary.wiley.com/doi/pdf/10.1002/anie.200502540>.
- <sup>12</sup>P. Li, Y. Jiao, J. Huang, and S. Chen, *JACS Au* **3**, 2640 (2023), <https://doi.org/10.1021/jacsau.3c00410>.
- <sup>13</sup>Z. K. Goldsmith, M. F. Calegari Andrade, and A. Selloni, *Chem. Sci.* **12**, 5865 (2021).
- <sup>14</sup>Y. R. Shen and V. Ostroverkhov, *Chemical Reviews* **106**, 1140 (2006), pMID: 16608175, <https://doi.org/10.1021/cr040377d>.
- <sup>15</sup>F. Perakis, L. De Marco, A. Shalit, F. Tang, Z. R. Kann, T. D. Kühne, R. Torre, M. Bonn, and Y. Nagata, *Chemical Reviews* **116**, 7590 (2016), pMID: 27096701, <https://doi.org/10.1021/acs.chemrev.5b00640>.
- <sup>16</sup>J.-J. Velasco-Velez, C. H. Wu, T. A. Pascal, L. F. Wan, J. Guo, D. Prendergast, and M. Salmeron, *Science* **346**, 831 (2014).
- <sup>17</sup>M. F. Toney, J. N. Howard, J. Richer, G. L. Borges, J. G. Gordon, O. R. Melroy, D. G. Wiesler, D. Yee, and L. B. Sorensen, *Nature* **368**, 444 (1994).
- <sup>18</sup>S. Nihonyanagi, S. Ye, K. Uosaki, L. Dreesen, C. Humbert, P. Thiry, and A. Peremans, *Surface Science* **573**, 11 (2004).
- <sup>19</sup>H. Noguchi, T. Okada, and K. Uosaki, *Faraday Discuss.* **140**, 125 (2009).
- <sup>20</sup>W.-T. Liu and Y. R. Shen, *Proceedings of the National Academy of Sciences* **111**, 1293 (2014).
- <sup>21</sup>Y. Tong, F. Lapointe, M. Thämer, M. Wolf, and R. K. Campen, *Angewandte Chemie International Edition* **56**, 4211 (2017), <https://onlinelibrary.wiley.com/doi/pdf/10.1002/anie.201612183>.
- <sup>22</sup>K. ichi Ataka, T. Yotsuyanagi, and M. Osawa, *The Journal of Physical Chemistry* **100**, 10664 (1996).
- <sup>23</sup>C.-Y. Li, J.-B. Le, Y.-H. Wang, S. Chen, Z.-L. Yang, J.-F. Li, J. Cheng, and Z.-Q. Tian, *Nature Materials* **18**, 697 (2019).
- <sup>24</sup>Y.-H. Wang, S. Zheng, W.-M. Yang, R.-Y. Zhou, Q.-F. He, P. Radjenovic, J.-C. Dong, S. Li, J. Zheng, Z.-L. Yang, G. Attard, F. Pan, Z.-Q. Tian, and J.-F. Li, *Nature* **600**, 81 (2021).
- <sup>25</sup>C.-Y. Li, J.-B. Le, Y.-H. Wang, S. Chen, Z.-L. Yang, J.-F. Li, J. Cheng, and Z.-Q. Tian, *Nature Materials* **18**, 697 (2019).
- <sup>26</sup>A. Poissier, S. Ganeshan, and M. V. Fernández-Serra, *Phys. Chem. Chem. Phys.* **13**, 3375 (2011).
- <sup>27</sup>L. S. Pedroza, A. Poissier, and M.-V. Fernández-Serra, *The Journal of Chemical Physics* **142**, 034706 (2015), [https://pubs.aip.org/aip/jcp/article-pdf/doi/10.1063/1.4905493/11052609/034706\\_1\\_online.pdf](https://pubs.aip.org/aip/jcp/article-pdf/doi/10.1063/1.4905493/11052609/034706_1_online.pdf).
- <sup>28</sup>A. Michaelides, V. A. Ranea, P. L. de Andres, and D. A. King, *Phys. Rev. Lett.* **90**, 216102 (2003).
- <sup>29</sup>S. Meng, E. G. Wang, and S. Gao, *Phys. Rev. B* **69**, 195404 (2004).
- <sup>30</sup>J.-B. Le, X.-H. Yang, Y.-B. Zhuang, M. Jia, and J. Cheng, *The Journal of Physical Chemistry Letters* **12**, 8924 (2021), pMID: 34499508, <https://doi.org/10.1021/acs.jpcclett.1c02086>.
- <sup>31</sup>R. Sundararaman, D. Vigil-Fowler, and K. Schwarz, *Chemical Reviews* **122**, 10651 (2022), pMID: 35522135, <https://doi.org/10.1021/acs.chemrev.1c00800>.
- <sup>32</sup>S. Sakong, J. Huang, M. Eikerling, and A. Groß, *Current Opinion in Electrochemistry* **33**, 100953 (2022).
- <sup>33</sup>J.-B. Le and J. Cheng, *Current Opinion in Electrochemistry Bioelectrochemistry*, fundamental and Theoretical Electrochemistry Bioelectrochemistry.
- <sup>34</sup>M. H. Hansen, C. Jin, K. S. Thygesen, and J. Rossmeisl, *The Journal of Physical Chemistry C* **120**, 13485 (2016), <https://doi.org/10.1021/acs.jpcc.6b00721>.
- <sup>35</sup>M. W. Swift, J. W. Swift, and Y. Qi, *Nature Computational Science* **1**, 212 (2021).
- <sup>36</sup>C. D. Taylor, S. A. Wasileski, J.-S. Filhol, and M. Neurock, *Phys. Rev. B* **73**, 165402 (2006).
- <sup>37</sup>J. Rossmeisl, J. K. Nørskov, C. D. Taylor, M. J. Janik, and M. Neurock, *The Journal of Physical Chemistry B* **110**, 21833 (2006), pMID: 17064147, <https://doi.org/10.1021/jp0631735>.
- <sup>38</sup>E. Skúlason, G. S. Karlberg, J. Rossmeisl, T. Bligaard, J. Greeley, H. Jónsson, and J. K. Nørskov, *Phys. Chem. Chem. Phys.* **9**, 3241 (2007).
- <sup>39</sup>S. Sakong, M. Naderian, K. Mathew, R. G. Hennig, and A. Groß, *The Journal of Chemical Physics* **142**, 234107 (2015), <https://doi.org/10.1063/1.4922615>.



- <sup>40</sup>S. Sakong and A. Groß, *The Journal of Chemical Physics* **149**, 084705 (2018), <https://doi.org/10.1063/1.5040056>.
- <sup>41</sup>G. Kastlunger, P. Lindgren, and A. A. Peterson, *The Journal of Physical Chemistry C* **122**, 12771 (2018), <https://doi.org/10.1021/acs.jpcc.8b02465>.
- <sup>42</sup>N. Bonnet, T. Morishita, O. Sugino, and M. Otani, *Phys. Rev. Lett.* **109**, 266101 (2012).
- <sup>43</sup>F. Deußenbeck, C. Freysoldt, M. Todorova, J. Neugebauer, and S. Wippermann, *Phys. Rev. Lett.* **126**, 136803 (2021).
- <sup>44</sup>L. S. Pedroza, P. Brandimarte, A. R. Rocha, and M.-V. Fernández-Serra, *Chem. Sci.* **9**, 62 (2018).
- <sup>45</sup>S. Datta, *Electronic Transport in Mesoscopic Systems*, Cambridge Studies in Semiconductor Physics and Microelectronic Engineering (Cambridge University Press, 1995).
- <sup>46</sup>A. R. Rocha, V. M. García-Suárez, S. Bailey, C. Lambert, J. Ferrer, and S. Sanvito, *Phys. Rev. B* **73**, 085414 (2006).
- <sup>47</sup>M. Brandbyge, J.-L. Mozos, P. Ordejón, J. Taylor, and K. Stokbro, *Phys. Rev. B* **65**, 165401 (2002).
- <sup>48</sup>N. Papior, G. Calogero, S. Leitherer, and M. Brandbyge, *Phys. Rev. B* **100**, 195417 (2019).
- <sup>49</sup>M. Bai, C. S. Cucinotta, Z. Jiang, H. Wang, Y. Wang, I. Rungger, S. Sanvito, and S. Hou, *Phys. Rev. B* **94**, 035411 (2016).
- <sup>50</sup>S. N. Rashkeev, M. Di Ventura, and S. T. Pantelides, *Phys. Rev. B* **66**, 033301 (2002).
- <sup>51</sup>R. Zhang, I. Rungger, S. Sanvito, and S. Hou, *Phys. Rev. B* **84**, 085445 (2011).
- <sup>52</sup>C. S. Ahart, S. K. Chulkov, and C. S. Cucinotta, *Journal of Chemical Theory and Computation* **0**, null (0), pMID: 39013589, <https://doi.org/10.1021/acs.jctc.4c00371>.
- <sup>53</sup>C. Caroli, R. Combescot, P. Nozieres, and D. Saint-James, *Journal of Physics C: Solid State Physics* **4**, 916 (1971).
- <sup>54</sup>J. M. Soler, E. Artacho, J. D. Gale, A. García, J. Junquera, P. Ordejón, and D. Sánchez-Portal, *Journal of Physics: Condensed Matter* **14**, 2745 (2002).
- <sup>55</sup>J. P. Perdew, K. Burke, and M. Ernzerhof, *Phys. Rev. Lett.* **77**, 3865 (1996).
- <sup>56</sup>N. Troullier and J. L. Martins, *Phys. Rev. B* **43**, 1993 (1991).
- <sup>57</sup>G.-C. Wang, S.-X. Tao, and X.-H. Bu, *Journal of Catalysis* **244**, 10 (2006).
- <sup>58</sup>J. Carrasco, J. Klimeš, and A. Michaelides, *The Journal of Chemical Physics* **138**, 024708 (2013), [https://pubs.aip.org/aip/jcp/article-pdf/doi/10.1063/1.4773901/14794398/024708\\_1\\_online.pdf](https://pubs.aip.org/aip/jcp/article-pdf/doi/10.1063/1.4773901/14794398/024708_1_online.pdf).
- <sup>59</sup>H. Deng, Y. Huang, and J. Li, *Langmuir* **39**, 11119 (2023), pMID: 37494475, <https://doi.org/10.1021/acs.langmuir.3c01545>.
- <sup>60</sup>K. Berland and P. Hyldgaard, *Physical Review B* **89**, 035412 (2014).
- <sup>61</sup>K. Fidanyan, G. Liu, and M. Rossi, *The Journal of Chemical Physics* **158**, 094707 (2023), [https://pubs.aip.org/aip/jcp/article-pdf/doi/10.1063/5.0139082/16791077/094707\\_1\\_online.pdf](https://pubs.aip.org/aip/jcp/article-pdf/doi/10.1063/5.0139082/16791077/094707_1_online.pdf).
- <sup>62</sup>S. Sakong and A. Groß, *Phys. Chem. Chem. Phys.* **22**, 10431 (2020).
- <sup>63</sup>R. Khatib, A. Kumar, S. Sanvito, M. Sulpizi, and C. S. Cucinotta, *Electrochimica Acta* **391**, 138875 (2021).
- <sup>64</sup>P. Li, J. Huang, Y. Hu, and S. Chen, *The Journal of Physical Chemistry C* **125**, 3972 (2021), <https://doi.org/10.1021/acs.jpcc.0c11089>.
- <sup>65</sup>S. Surendralal, M. Todorova, and J. Neugebauer, *Phys. Rev. Lett.* **126**, 166802 (2021).
- <sup>66</sup>J. Carrasco, A. Hodgson, and A. Michaelides, *Nature Materials* **11**, 667 (2012).
- <sup>67</sup>T. Seki, K.-Y. Chiang, C.-C. Yu, X. Yu, M. Okuno, J. Hunger, Y. Nagata, and M. Bonn, *The Journal of Physical Chemistry Letters* **11**, 8459 (2020), pMID: 32931284, <https://doi.org/10.1021/acs.jpclett.0c01259>.
- <sup>68</sup>Z. K. Goldsmith, M. Secor, and S. Hammes-Schiffer, *ACS Central Science* **6**, 304 (2020), pMID: 32123749.
- <sup>69</sup>Y. Tong, F. Lapointe, M. Thämer, M. Wolf, and R. K. Campen, *Angewandte Chemie International Edition* **56**, 4211 (2017), <https://onlinelibrary.wiley.com/doi/pdf/10.1002/anie.201612183>.
- <sup>70</sup>A. J. Tursi and E. R. Nixon, *The Journal of Chemical Physics* **52**, 1521 (1970), <https://doi.org/10.1063/1.1673163>.
- <sup>71</sup>J.-S. Filhol and M. Neurock, *Angewandte Chemie International Edition* **45**, 402 (2006), <https://onlinelibrary.wiley.com/doi/pdf/10.1002/anie.200502540>.
- <sup>72</sup>J. I. Siepmann and M. Sprik, *The Journal of Chemical Physics* **102**, 511 (1995), <https://doi.org/10.1063/1.469429>.
- <sup>73</sup>Y. Zhang, H. B. de Aguiar, J. T. Hynes, and D. Laage, *The Journal of Physical Chemistry Letters* **11**, 624 (2020), pMID: 31899643, <https://doi.org/10.1021/acs.jpclett.9b02924>.
- <sup>74</sup>L. D. Burke, *Gold Bulletin* **37**, 125 (2004).
- <sup>75</sup>B. D. Adams and A. Chen, *Materials Today* **14**, 282 (2011).